Chaos, Solitons and Fractals 139 (2020) 110094

Contents lists available at ScienceDirect

Chaos, Solitons and Fractals

Nonlinear Science, and Nonequilibrium and Complex Phenomena

journal homepage: www.elsevier.com/locate/chaos

Quantitative study of the relative effects of initial condition and model uncertainties on local predictability in a nonlinear dynamical system

Xuan Li [a], Ruiqiang Ding [b,*], Jianping Li [c]

[a] Department of Atmospheric and Oceanic Sciences and Institute of Atmospheric Sciences, Fudan University, Shanghai, 200438, China
[b] State Key Laboratory of Earth Surface Processes and Resource Ecology, Beijing Normal University, Beijing 100875, China
[c] Key Laboratory of Physical Oceanography/Institute for Advanced Ocean Studies, Ocean University of China and Qingdao National Laboratory for Marine Science and Technology, Qingdao 266100, China

ARTICLE INFO

Article history:
Received 29 December 2019
Revised 29 June 2020
Accepted 4 July 2020

Keywords:
Initial condition and model uncertainties
Nonlinear local Lyapunov exponent
Local predictability limit
Inverse spatial distributions

ABSTRACT

The relative effects of initial condition and model uncertainties on local predictability are important issues in the atmospheric sciences. This study quantitatively compared the relative effects of these two types of uncertainty on local predictability using the Lorenz model. Local predictability limits were quantitatively estimated using the nonlinear local Lyapunov exponent (NLLE) method. Results show that the relative effects of initial conditions and model uncertainties on local predictability vary with the state. In addition, inverse spatial distributions of local predictability limits are induced by the two types of uncertainty. In the regime transition region, the local predictability limits of modeled states are more sensitive to initial condition uncertainty than to model uncertainty, resulting in lower local predictability limits being induced by initial condition uncertainties. Local predictability limits induced by initial condition uncertainties are 4 time units shorter than those induced by model uncertainties. In the "butterfly wing" regions, the local predictability limits of modeled states are more sensitive to model uncertainty than to initial condition uncertainty, resulting in lower local predictability limits due to model uncertainty. Local predictability limits induced by initial condition uncertainty are larger (0 to 4 time units) than those induced by model uncertainty. These differences in the regions that are sensitive to the two types of uncertainty mean that strategic reductions of uncertainty in sensitive areas may effectively improve forecast skill.

1. Introduction

Models of the atmosphere, a hyper-chaotic system, are extremely sensitive to initial conditions. Small errors between initially adjacent trajectories grow rapidly and quickly affect the whole attractor. Consequently, forecasting accuracy decreases rapidly to the point of being meaningless. Thus, accurate forecasts of the atmosphere are always challenging. Two main contributors to this loss of predictability are uncertainties in the initial conditions and in the model [5,7,39,76,77,79]. In the atmospheric system, slight differences between observed and true state values are inevitable, even with the application of advanced observation techniques and data assimilation methods. Initial condition uncertainty is therefore unavoidable. In addition, incomplete understanding of atmospheric dynamics, parameterizations of subgrid scale microphysical processes and low model resolution result in model uncertainty. These two types of uncertainty influence the predictability of the atmosphere. Lorenz [39] used them to classify predictability as related mainly to either to initial condition uncertainty or to model uncertainty. Many works have studied the effects of the two types of uncertainty on the two types of predictability [17,19,23,31,33,47,48,65,75].

Since the pioneering work of Thompson [66] and Lorenz [35], much research on the influence of initial errors on predictability has been performed. Predictability is closely related to the growth rate of the initial error. When the initial errors evolve to exceed a certain threshold value, predictability can be considered to be lost [8,42,49,62,70]. Lorenz [36] first investigated the growth of error systematically in a "low-order" model with 28 variables. This study demonstrated that the error growth was highly dependent on synoptic conditions, and atmospheric predictability reached approximately four days, during which time small errors doubled in magnitude. Later, Lorenz [37] investigated error growth by searching for analogues in observational data. Lorenz pointed out that small initial errors among analogues would grow at a quasi-exponential

* Corresponding author.
E-mail address: drq@mail.iap.ac.cn (R. Ding).

https://doi.org/10.1016/j.chaos.2020.110094
0960-0779/

rate at the early stage. After the early stage, the growth rate would decrease to zero and the error growth would effectively stop because of nonlinear terms in the dynamical equations. Lorenz assumed the nonlinear terms to be quadratic, although this was not readily proved. According to this quadratic hypothesis, small errors would double in ~2.5 days. Trevisan [67] studied the rate of error growth at the transient stage, and pointed out that the growth rate during the transient period could great affect predictability with initial errors of a given finite size. Based on previous studies of various error growth rates at different stages [21,29], Lorenz [43] proposed three possible stages for the error growth rate: an early stage with rapid growth, a mature stage with quasi-exponential growth and a saturation stage with zero growth. In addition to the error growth rate, the initial error size also affects the predictability. Lorenz [38] pointed out that the predictability limit can be increased by reducing the initial error size in chaotic systems. Ding and Li [9] applied the nonlinear finite-time Lyapunov exponent (FTLE) for chaotic systems to study the impact of initial error size on predictability. According to this study, the predictability limit decreased as the infinitesimally small error size in chaotic systems increased. Therefore, reducing initial errors by increasing the observations in sensitive areas and applying data assimilation techniques are effective methods for improving forecasting [1,18,51,71,78].

In addition to initial condition uncertainty, model uncertainty also affects the predictability of the atmosphere. The impacts of model uncertainty on predictability receive less attention than do those of initial condition uncertainty. However, previous studies have pointed out that model errors have a great influence on predictability, and should not be ignored (e.g., [7,26,58]). Although model uncertainty contributes to the loss of predictability, its dynamics are still unclear. Leith [30] proposed an empirical equation describing the growth of uncertainties combining both uncertainty types. It implied that the model error growth is linear for a short time when no initial errors are present in the system. However, Vannitsem and Toth [69] studied the short-term dynamics of model errors in a low-order atmospheric system [40] and suggested that the quadratic evolution of model error growth is common. Zhu and Thorpe [79] investigated the influence of model uncertainty on the predictability of extratropical cyclones. Their study found that the model uncertainty growth increased as time to the power μ ranged from 0.5 to 3 during the early period, when no initial errors were present. After a certain time, the model uncertainty growth reached a saturation value. The time for model uncertainty to enter the saturation stage is associated with the intensity of the cyclone. The greater the intensity, the less time it takes to reach saturation. Therefore, reducing model uncertainty can improve forecasting. Multi-model ensemble forecasting is a commonly used method to reduce model uncertainty [3,24,28,60,64].

Both types of uncertainty influence predictability, but which has the larger impact? It is widely recognized that initial condition uncertainty plays a more important role in short-range forecasts, whereas in extended-range forecasts model uncertainty dominates [41]. Researchers have compared the relative roles of initial condition and boundary uncertainties in predictability using operational analysis (e.g., [16,61]), finding a greater contribution to forecast errors by initial condition uncertainty. However, other studies have found that initial condition and boundary condition uncertainties are comparably important, and should both be taken into account (e.g., [7,26]). Chu [6] adopted the Lorenz model to investigate the sensitivity of predictability to initial condition and model uncertainties. This study found that model uncertainty had an effect on atmospheric predictability comparable to that of initial condition uncertainty, and thus model uncertainty should not be ignored. In addition, Orrell et al. [56] applied the local model drift approach to quantify state-dependent model error, and found that model uncertainty dominated the growth of forecast errors for up to 3 days.

It is of great significance to study the relative effects of initial condition and model uncertainties. These efforts can contribute to the improvement of forecast skill for weather and climate events occurring in some local regions by reducing the corresponding uncertainties to which such events are sensitive [2,4,44,50,51]. Although much research has studied the relative effects of the two types of uncertainty on local predictability, a consensus has not yet been reached. Moreover, previous studies have focused on qualitative comparisons of the impacts of the two types of uncertainty on local predictability. Quantitative comparisons have not yet been reported. Chu [6] investigated only one set of initial conditions, and did not provide a quantitative comparison of the relative effects of the two types of uncertainty on local predictability.

The purpose of this work is to study and quantitatively compare the relative effects of the two types of uncertainty on local predictability. We followed the approach of Chu [6], but considered more initial states for the attractor. Previous studies used the local Lyapunov exponent (LLE) method to analyze the local predictability of chaotic systems [53,74]. The LLEs characterize average growth rates of infinitesimally small errors in the linear phase. However, when the errors grow to a certain size, the LLE method is not applicable. The nonlinear local Lyapunov exponent (NLLE, [9,12,34]) measures the average growth rates of errors in dynamical systems without linearizing the governing equations. Consequently, the NLLE method remains practicable even when the errors grow to a certain size, which is an advantage over the LLE method. Therefore, we used the NLLE method to estimate the local predictability limits induced by initial condition and model uncertainties. The relative effects of the two types of uncertainty were quantitatively compared by calculating differences in the local predictability limits. The remainder of this paper is arranged as follows. Section 2 introduces the model, the NLLE method, and the experimental design. The results of a quantitative comparison of the relative effects of the two types of uncertainty on local predictability limits are described in Section 3. Finally, a discussion and conclusions are presented in Section 4.

2. Model and method

2.1. Model description

Lorenz [35] designed a simplified mathematical model to study atmospheric convection. It contains three nonlinear ordinary differential equations:

$$\begin{cases} \dot{x} = -\sigma(x - y) \\ \dot{y} = -xz + rx - y, \\ \dot{z} = xy - bz \end{cases} \tag{1}$$

where σ, r, and b are three parameters set to 10, 28, and 8/3, respectively, in the Lorenz model, which exhibits chaotic behavior. The Lorenz model has been widely used in meteorological science studies as it can reveal some features of the real atmosphere, such as the sensitivity to initial conditions and various properties of quasi-stationary regimes [20,45,57,59,72]. Projections of the Lorenz attractor on two-dimensional planes are shown in Fig. 1. As shown in Fig. 1b, the attractor has a shape similar to that of a butterfly, so the Lorenz attractor is also referred to as the butterfly attractor.

2.2. NLLE method

A large number of studies [21,27,36,46,52,53,68,73,74,80] have investigated atmospheric predictability by measuring error growth in the context of linear error dynamics. It is assumed that the initial error size is infinitesimal and the integration time is short.

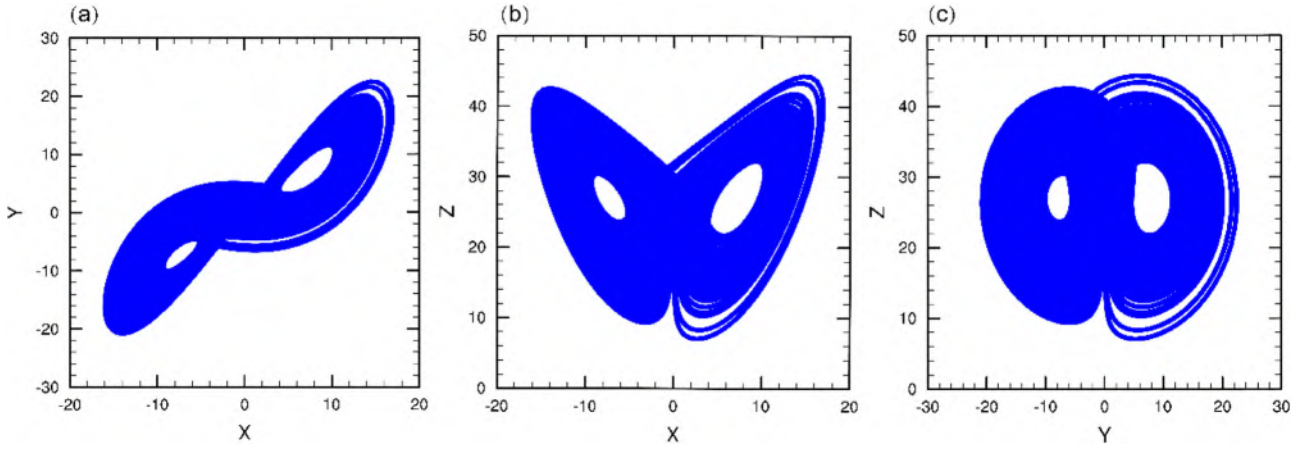

Fig. 1. Projections of the Lorenz attractor on three two-dimensional planes: the (a) X–Y, (b) X–Z, and (c) Y–Z planes.

However, the magnitude of the initial error generally has a finite size in models of the real atmosphere, and the initial error growth is affected by nonlinear effects over time. Therefore, investigations of atmospheric predictability using linear error dynamics theory are of limited value. Ding and Li [9] and Ding et al. [12] proposed the NLLE method to study atmospheric predictability by measuring the nonlinear growth of initial errors of a finite size without linearizing the equation. The NLLE method accounts for nonlinear effects, and has been successfully applied in the field of atmospheric and oceanic predictability [10,11,13,15,22]. A description of the NLLE method follows.

In an n-dimensional nonlinear system, the dynamics are governed by

$$\frac{d}{dt}\boldsymbol{x}(t) = F[\boldsymbol{x}(t)], \tag{2}$$

where $\boldsymbol{x}(t) = (x_1(t), x_2(t), \ldots x_n(t))^T$ is the state vector. The evolution of initial perturbations $\delta(t_0)$ can be described by

$$\boldsymbol{\delta}(t_0+\tau) = \boldsymbol{\eta}\big(\boldsymbol{x}(t_0), \boldsymbol{\delta}(t_0), \tau\big)\delta(t_0), \tag{3}$$

where $\boldsymbol{\delta}(t) = (\delta_1(t), \delta_2(t), \ldots \delta_n(t))^T$ represents perturbations at time t, and $\boldsymbol{\eta}(\boldsymbol{x}(t_0), \boldsymbol{\delta}(t_0), \tau)$ is the nonlinear error propagator that propagates the initial perturbation $\boldsymbol{\delta}(t_0)$ forward to perturbation $\boldsymbol{\delta}(t)$. The NLLE is defined as

$$\lambda\big(\boldsymbol{x}(t_0), \quad \boldsymbol{\delta}(t_0), \tau\big) \;=\; \frac{1}{\tau}\ln\frac{\|\delta(t_0+\tau)\|}{\|\delta(t_0)\|}, \tag{4}$$

where $\lambda(\boldsymbol{x}(t_0), \boldsymbol{\delta}(t_0), \tau)$ depends on the initial state $\boldsymbol{x}(t_0)$ in phase space, the initial perturbation $\boldsymbol{\delta}(t_0)$, and the integration time τ. The NLLE represents the average nonlinear growth rate of initial errors evolving from t_0 to $t_0+\tau$.

For a state $\boldsymbol{x}(t_0)$ in phase space, if a group of error vectors of the same infinitesimal magnitude but different direction are centered on this state (as shown in Fig. 2), the NLLE of each dimension can be given by

$$\lambda_i\big(\boldsymbol{x}(t_0), \boldsymbol{\delta}(t_0), \tau\big) = \frac{1}{\tau}\ln\frac{\|\delta_i(t_0+\tau)\|}{\|\delta_i(t_0)\|}, \tag{5}$$

where $\delta_i(t_0+\tau)$ is the error of the i-th dimension at $t_0+\tau$, and $\lambda_i(\boldsymbol{x}(t_0), \boldsymbol{\delta}(t_0), \tau)$ is the NLLE of the i-th dimension. The ensemble mean NLLE of an n-dimensional "error ball" can be expressed by

$$\bar{\lambda}(\boldsymbol{x}(t_0), \tau) = \big\langle \lambda_i\big(\boldsymbol{x}(t_0), \boldsymbol{\delta}(t_0), \tau\big)\big\rangle_n, \tag{6}$$

where $\langle\,\rangle_n$ indicates an ensemble average of a multi-dimensional NLLE whose size is n. Therefore, the mean local relative error growth superposed on $\boldsymbol{x}(t_0)$ can be obtained by

$$\bar{E}(\boldsymbol{x}(t_0), \tau) = \exp\big(\bar{\boldsymbol{\lambda}}(\boldsymbol{x}(t_0), \tau)\tau\big). \tag{7}$$

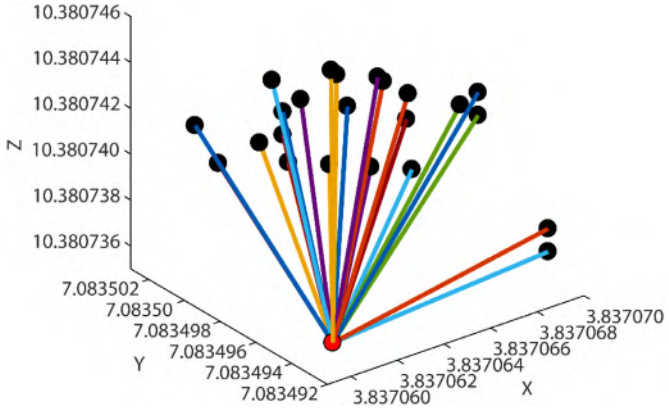

Fig. 2. Example of 25 error vectors superimposed on state $x(t_0)$. The red dot represents the state $x(t_0)$, and the lines connecting the red and black dots represent the error size. The magnitude of the error vectors is 10^{-5}.

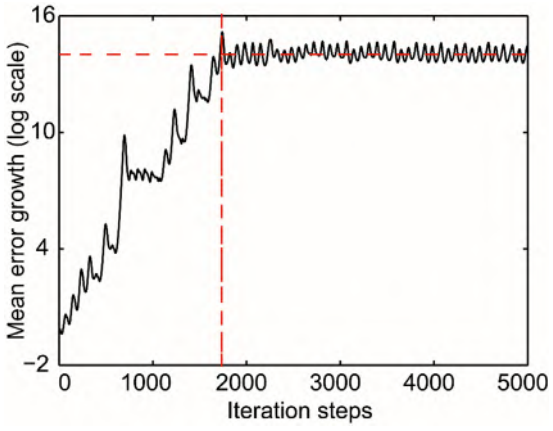

Fig. 3. Ensemble mean of the logarithmic error growth as a function of iteration step.

The error growth $\bar{E}(\boldsymbol{x}(t_0), \tau)$ is a function of time. It will reach a saturation level and cease to grow over time. The predictability limit of a single state $\boldsymbol{x}(t_0)$ in phase space can be measured by the time when the forecast error exceeds 95% of the saturation value [8,13,14,25,32,63].

Fig. 3 shows an example of the estimation of the predictability limit of a single state in the Lorenz model using the NLLE method. The single state is (−0.61, 2.66, 27.9) and the magnitude of the ini-

tial error is 10^{-5}. As shown in Fig. 3, the initial errors grow erratically with time at first. After ~1800 iteration steps, nonlinearity dominates the growth of errors and the errors cease to grow but fluctuate around a saturation value at which point the initial information and predictability of the state are lost. The predictability of the state can be estimated quantitatively as 17 ($1800 \times 0.01 \times 95\%$) time units. The local predictability limit, 17 time units, represents the longest prediction time from the initial state (−0.61, 2.66, 27.9).

2.3. Experiment design

The initial state is given as (1.0, −0.3, 1.2). We integrated the Lorenz model for 105,000 time steps using a fourth-order Runge–Kutta scheme with a time step, Δt, of 0.01 time units. The first 5000 time steps are discarded for spin-up with the remaining 100,000 states used to represent the "true" system. These states are used to investigate the relative effects of initial condition and model uncertainties on local predictability. We performed model runs for two different scenarios. One model run has only initial errors (i.e., no model error exists in the system). The other has only model errors, with no initial errors. To ensure a fair comparison of the relative effects of the two types of uncertainty on local predictability, the initial condition and model uncertainties superimposed on the same state are always of the same magnitude.

2.3.1. Scenario one: only initial condition errors

Consider $(\boldsymbol{x}(t_0), \boldsymbol{y}(t_0), \boldsymbol{z}(t_0))$ to be a true state in phase space. A group of initial error vectors are superimposed on this state. The directions of the initial error vectors are different but their magnitudes all equal $\boldsymbol{\delta}$. An imperfect state $(\boldsymbol{x}'(t_0), \boldsymbol{y}'(t_0), \boldsymbol{z}'(t_0))$ can then be represented by

$$\boldsymbol{x}'(t_0) = \boldsymbol{x}(t_0) + \boldsymbol{\delta}_1, \tag{8}$$

$$\boldsymbol{y}'(t_0) = \boldsymbol{y}(t_0) + \boldsymbol{\delta}_2, \tag{9}$$

$$\boldsymbol{z}'(t_0) = \boldsymbol{z}(t_0) + \boldsymbol{\delta}_3, \tag{10}$$

$$\boldsymbol{\delta}^2 = \boldsymbol{\delta}_1^2 + \boldsymbol{\delta}_2^2 + \boldsymbol{\delta}_3^2, \tag{11}$$

where $\boldsymbol{\delta}_1$, $\boldsymbol{\delta}_2$, and $\boldsymbol{\delta}_3$ are the three components of the initial error vectors $\boldsymbol{\delta}$ superimposed in the *x*, *y*, and *z* directions, respectively. The true state $(\boldsymbol{x}(t_0), \boldsymbol{y}(t_0), \boldsymbol{z}(t_0))$ and the imperfect states $(\boldsymbol{x}'(t_0), \boldsymbol{y}'(t_0), \boldsymbol{z}'(t_0))$ are integrated for 5000 time steps as a true run and a forecast run, respectively. The forecast error can be obtained by calculating the difference of the forecast run and true run. Using the NLLE method, the predictability limit of state $(\boldsymbol{x}(t_0), \boldsymbol{y}(t_0), \boldsymbol{z}(t_0))$ induced by initial condition uncertainty can be determined quantitatively.

2.3.2. Scenario two: only model errors

For the scenario with model errors but no initial condition errors, the three parameters are regarded as state variables. Then, a group of model error vectors are superimposed on the three parameters. The system can thus be represented by

$$\sigma' = \sigma + \boldsymbol{\varepsilon}_1, \tag{12}$$

$$b' = b + \boldsymbol{\varepsilon}_2, \tag{13}$$

$$r' = r + \boldsymbol{\varepsilon}_3, \tag{14}$$

$$\boldsymbol{\varepsilon}^2 = \boldsymbol{\varepsilon}_1^2 + \boldsymbol{\varepsilon}_2^2 + \boldsymbol{\varepsilon}_3^2, \tag{15}$$

where ε_1, ε_2, and ε_3 are the three components of initial vectors ε superimposed on parameters σ, b, and r, respectively. To explore the effect of model uncertainty on the predictability of state $(\boldsymbol{x}(t_0), \boldsymbol{y}(t_0), \boldsymbol{z}(t_0))$, we integrate the perfect model and the imperfect model for 5000 time steps from state $(\boldsymbol{x}(t_0), \boldsymbol{y}(t_0), \boldsymbol{z}(t_0))$ as a true run and a forecast run, respectively. Using the NLLE method, the predictability limit of state $(\boldsymbol{x}(t_0), \boldsymbol{y}(t_0), \boldsymbol{z}(t_0))$ induced by model uncertainty can be determined quantitatively by studying the growth of the model error.

3. Results

The relative effects of initial condition and model uncertainties on local predictability can be quantified by comparing the local predictability limits of states induced by the two types of uncertainty. The local predictability limits depend on the growth rates and sizes of the errors. Before comparing the relative effects of the two types of error, their growth rates are explored. We calculate the error rate as

$$\lambda = \frac{1}{t - t_0} \ln \frac{\| \Delta x(t) \|}{\| \Delta x(t_0) \|}, \tag{16}$$

where t_0 and t denote the initial and evolution times, respectively, and $\Delta \boldsymbol{x}(t_0)$ and $\Delta \boldsymbol{x}(t)$ represent the magnitude of uncertainty at t_0 and t, respectively. Two groups of 10,000 initial condition and model error vectors of the same magnitude but different direction were superimposed on the states under the two scenarios. At each iteration step, we averaged the growth of all error vectors to obtain the average growth of errors within the iteration steps. A large number of cases of states was chosen in our work. Under scenario one, the true state $(\boldsymbol{x}(t_0), \boldsymbol{y}(t_0), \boldsymbol{z}(t_0))$ and imperfect states $(\boldsymbol{x}'(t_0), \boldsymbol{y}'(t_0), \boldsymbol{z}'(t_0))$ are integrated for 5000 time steps as a true run and a forecast run, respectively. Under scenario two, we integrated the perfect and imperfect model for 5000 time steps from the same state $(\boldsymbol{x}(t_0), \boldsymbol{y}(t_0), \boldsymbol{z}(t_0))$ as a true run and a forecast run, respectively. The growth rates of the initial condition and model uncertainties with iteration steps can then be obtained using Eq. 16. The relative growth rates of the initial condition and model errors are thus found to vary with phase and state. Fig. 4 shows the growth rates of the initial condition and model errors for three cases. The three different states are (11.91, 9.96, 34.64), (3.89, 6.47, 14.66) and (1.53, 1.07, 22.25). The magnitudes of the initial condition and model uncertainties are both 10^{-2}. As shown in Fig. 4, the growth rates of the two types of error rapidly reach a maximum value (in ~100 iterations). Afterwards, the growth rates both decrease rapidly. The growth rates of the initial condition and model errors generally differ during the first 1000 iteration steps. After which, the growth rates are the same. During the first 1000 iteration steps, the relative growth rates of the initial condition and model errors are still variable (e.g., Fig. 4c).

The corresponding error growth of the initial condition and model uncertainties superimposed on these three states are shown in Fig. 5, where it is evident that the error first increases in a zigzag pattern. After some time, the error ceases to grow and fluctuates with a relatively small amplitude. The phase when the error ceases to grow is the saturation period. We calculated the average value of the magnitudes of the errors in the period of saturation as the saturation level. For the first state (11.91, 9.96, 34.64), the growth rate of the model error is always higher than that of the initial error during the first 500 iteration steps (Fig. 4a). In this phase, the growth rate of the model error is larger and hence reaches saturation faster than does the initial error (Fig. 5a). For the second state (3.89, 6.47, 14.66), the growth rate of the model error is initially less than that of the initial error. However, after some time, the growth rate of the initial error increases, and the two types of error eventually reach saturation at the same time

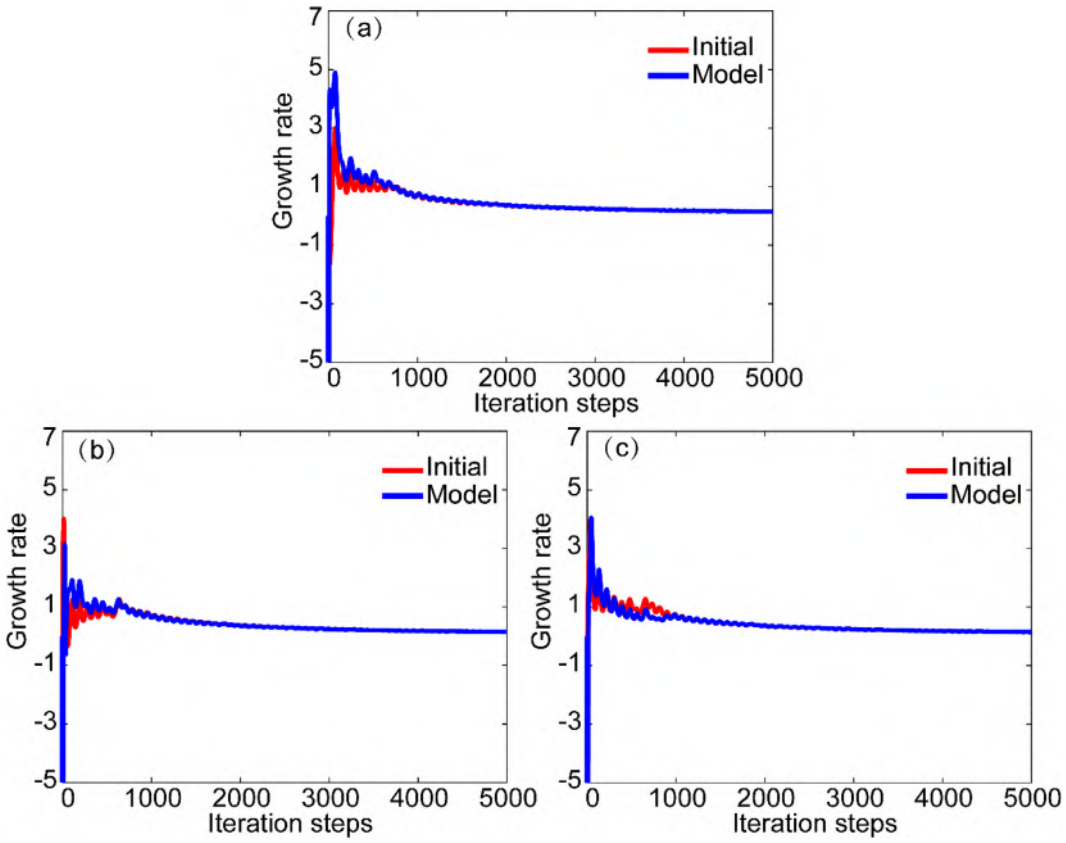

Fig. 4. Comparison of growth rates for initial (red) and model (blue) errors by iteration step for three unique states: (a) (11.91, 9.96, 34.64), (b) (3.89, 6.47, 14.66), and (c) (1.53, 1.07, 22.25). The magnitudes of the initial condition and model uncertainties are both 10^{-2}. (For interpretation of the references to color in this figure legend, the reader is referred to the web version of this article.)

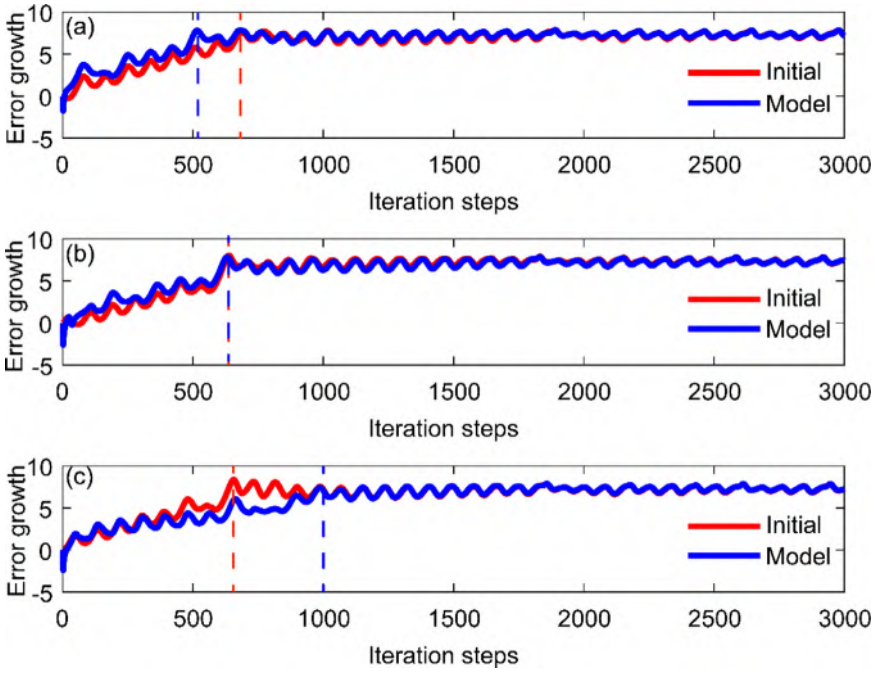

Fig. 5. As Fig. 4, but for the growth of initial condition and model uncertainties. The red (blue) dashed line denotes the time when the initial (model) error reaches saturation. (For interpretation of the references to color in this figure legend, the reader is referred to the web version of this article.)

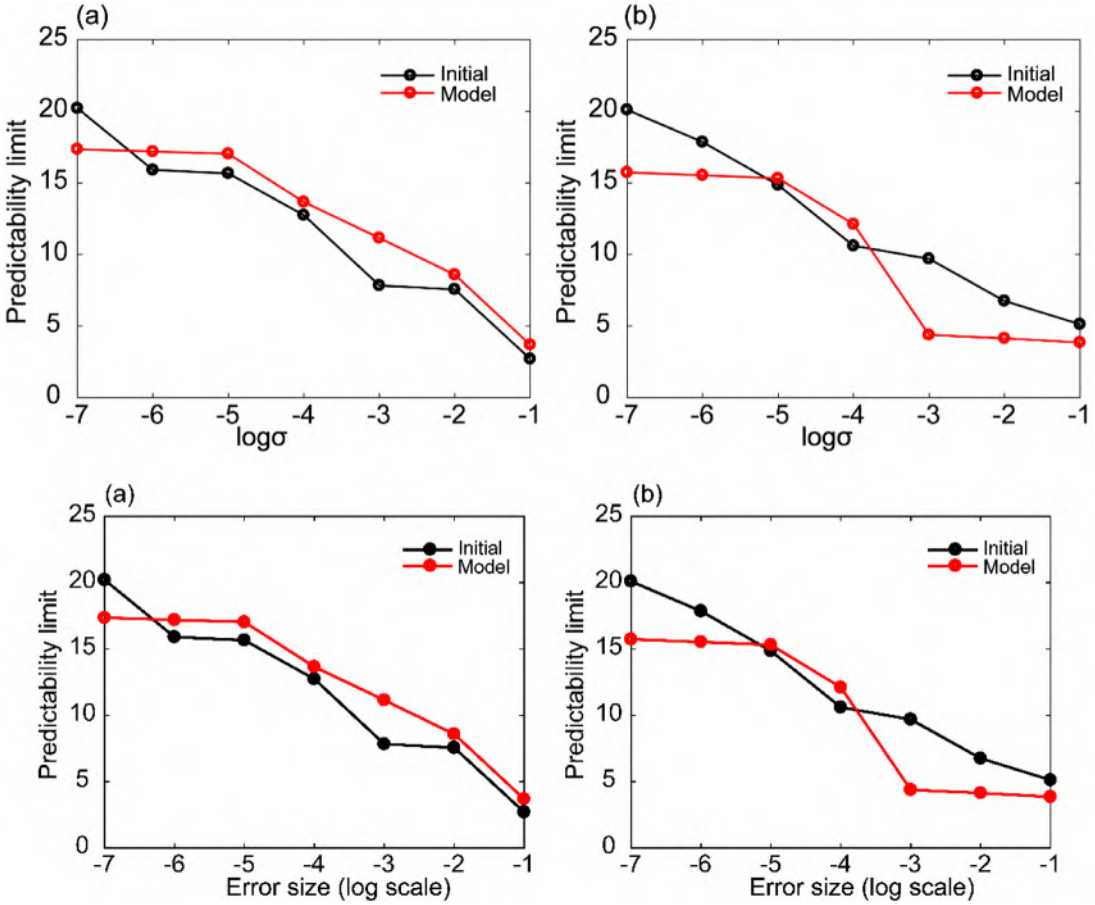

Fig. 6. Variation of predictability limits for initial condition and model uncertainties for unique states (a) (−0.96, 2.68, 28.5) and (b) (8.39, 1.05, 36.20). The black (red) line denotes the initial condition (model) uncertainty. (For interpretation of the references to color in this figure legend, the reader is referred to the web version of this article.)

(Fig. 5b). For the third state (1.53, 1.07, 22.25), to begin with, the growth rate of the model error is slightly lower than that of the initial error. After some time, the initial error grows more rapidly than does the model error, and eventually saturates faster (Fig. 5c). As the time to saturation for the initial condition and model errors differ among the states, the relative effects of the two types of uncertainty vary with state as well.

To quantify the relative effects of initial condition and model uncertainties on local predictability, we first estimated the local predictability limits of the states induced by these two types of uncertainty. Fig. 6 shows the variation of local predictability limits of two different states with the magnitude of the initial condition and model uncertainties. The two states are (−0.96, 2.68, 28.5) and (8.39, 1.05, 36.20). The magnitudes of the initial condition and model uncertainties range from 10^{-7} to 10^{-1}. As shown in Fig. 6a and b, the local predictability limits of these two states both decrease as the magnitude of uncertainty increases regardless of which type of uncertainty is present. This indicates that both initial condition and model uncertainties have negative effects on local predictability.

The Lorenz model has three parametersσ, r, and b, which impact local predictability limits; we also considered the sensitivities of local predictability limits to these parameters. In this scenario, no initial condition error is present in the model and only the parameter uncertainties are present. To study the sensitivity of the predictability of the Lorenz system to each parameter, the parameter error was superimposed on one parameter, while the other two parameters remained accurate and fixed. We selected 10,000 consecutive but different initial conditions to perform the experiment. For each initial condition, we integrated the perfect and imperfect models for 5000 time steps. Then we computed the ensemble mean of the error growths for all 10,000 initial conditions at each iteration step. Based on the time that the average errors reach saturation, we estimated the predictability limit induced by only one type of parameter uncertainty. Fig. 7 shows the variations of predictability limits for each parameter uncertainty at different magnitudes, indicating that predictability limits decrease as the magnitudes of the parameter uncertainties increase. In addition, for the same magnitude of uncertainties of the three parameters, the predictability limits induced by parameter σ are always higher than those induced by the other two parameters. The predictability limits induced by parameter b are the lowest. These results indicate that the uncertainty of parameter b has the largest impact on the predictability limits, and uncertainty of parameter σ the least impact. Therefore, the local predictabilities are most sensitive to parameter b, less sensitive to parameter r, and least sensitive to parameter σ.

We next select a trajectory including 500 consecutive states (Fig. 8a) and calculate their local predictability limits induced by initial condition and model uncertainties. Fig. 8b shows the local predictability limits of the 500 consecutive states. The magnitudes of the initial condition and model uncertainties are both 10^{-2}. As evident in Fig. 8b, the local predictability limits vary with state regardless of which type of uncertainty is imposed in the system. In some cases, the local predictability limits of states induced by initial condition and model uncertainties are the same. However, in most cases, the local predictability limits induced by the two types of uncertainty are different. This variation of local predictability

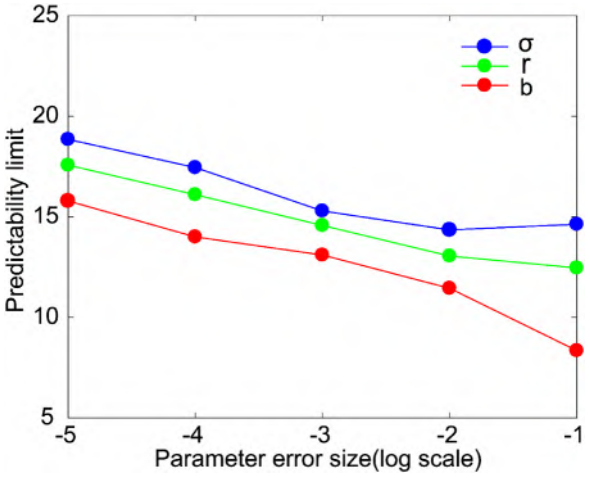

Fig. 7. Variation of predictability limits for uncertainties associated with the three parameters (σ, r, and b) with different magnitudes. The blue, green, and red colors represent the uncertainties of σ, r, and b, respectively. The base of the logarithm function is 10. (For interpretation of the references to color in this figure legend, the reader is referred to the web version of this article.)

limits indicates that the relative contributions of initial condition and model uncertainties to loss of predictability depend on the chosen states.

To quantify the relative roles of initial condition and model uncertainties in local predictability limits of states on the attractor, we calculate the differences between the local predictability limits of the same states induced by the two types of uncertainty. When the local predictability limit of a single state induced by initial condition errors is higher than that induced by model errors, it means that model errors have a more negative effect on local predictability than do initial condition errors, and vice versa. When the local predictability limits induced by initial condition and model errors are equal, it means that the initial condition and model errors have the same effects on local predictability. Therefore, a quantitative comparison of the relative effects of initial condition and model errors on local predictability can be obtained by calculating the difference between the predictability limits induced by initial condition and model errors. Fig. 9 shows the differences between predictability limits induced by initial condition and model errors with magnitudes of 10^{-2} and 10^{-5}. As shown in Fig. 9a and b, the differences in the predictability limits of 500 consecutive states induced by initial condition and model errors fluctuate around zero, suggesting that the relative effects of initial condition and model uncertainties vary with state. In addition, the differences appear to change periodically with time. The difference increases with time and gradually reaches a peak value. After this peak, the difference decreases with time to a minimum value below zero. Subsequently, this cycle of variations of the difference repeats.

To determine the origin of this phenomenon, more consecutive states are evaluated. Fig. 10 shows the spatial distributions and the differences of local predictability limits of 2000 states induced by initial condition and model errors with magnitudes of 10^{-2} and 10^{-5}. As shown in Fig. 10a and d, the predictability limits of states on the "butterfly wing" regions are generally higher, and the predictability limits of states on the regime transition region are lower. As the magnitudes of the initial condition and model uncertainties superimposed on each state are of the same magnitude, this suggests that the local predictabilities in the regime transition region are sensitive to initial condition uncertainty. The growth rate of initial condition uncertainty is thus faster, which results in less time for it to reach saturation. In the "butterfly wing" regions of the attractor, the local predictability is relatively insensitive to initial condition uncertainty, leading the initial condition uncertainty to slowly reach saturation. The spatial distributions of local predictability limits of states induced by model uncertainties are shown in Fig. 10b and e. Unlike the spatial distributions of predictability limits induced by initial condition uncertainties, the local predictability limits of states in the regime transition region are higher and the predictability limits of states in the "butterfly wing" regions are lower. This indicates that local predictabilities in the regime transition region are insensitive to model uncertainty, whereas local predictabilities in the "butterfly wing" regions are more sensitive to model uncertainty. The growth rates of model uncertainties in the "butterfly wing" regions are thus faster and more quickly reach saturation. In the regime transition region, local predictability is insensitive to model uncertainty, leading to more time for model uncertainties to reach saturation. Fig. 10c and f shows the differences between the local predictability limits induced by initial condition and model errors. The differences in the regime transition region are negative, suggesting that initial condition uncertainties have a more negative effect on local predictability than do model uncertainties. Additionally, the difference values are approximately −4, indicating that forecasts can be 4 time units longer in the scenario with model uncertainty than in the scenario with initial condition uncertainty, both of which have the same magnitudes of uncertainty in this region. The difference values are the same for all uncertainty magnitudes. In the "butterfly wing" regions, the differences are positive, indicating that model uncertainties play a more negative role in local predictability in these regions. The difference values are up to 4, with positive values accounting for the ma-

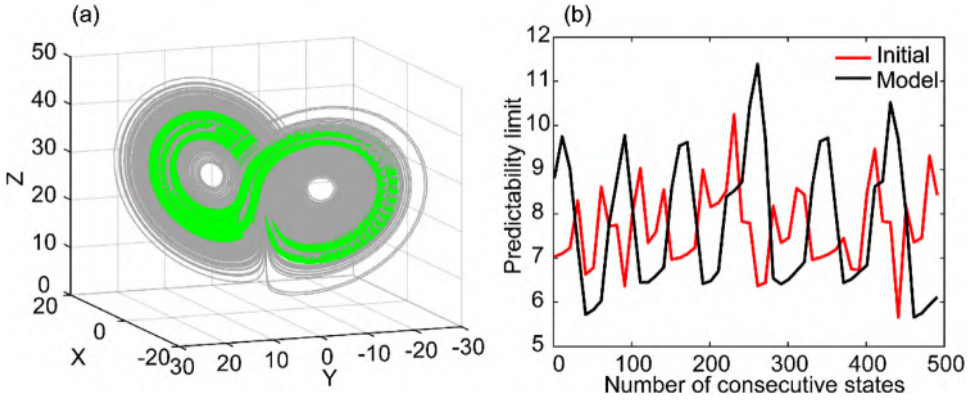

Fig. 8. (a) Trajectory (green line) for 500 consecutive states on the attractor, and (b) predictability limits of 500 consecutive states induced by initial (red) and model (black) errors. (For interpretation of the references to color in this figure legend, the reader is referred to the web version of this article.)

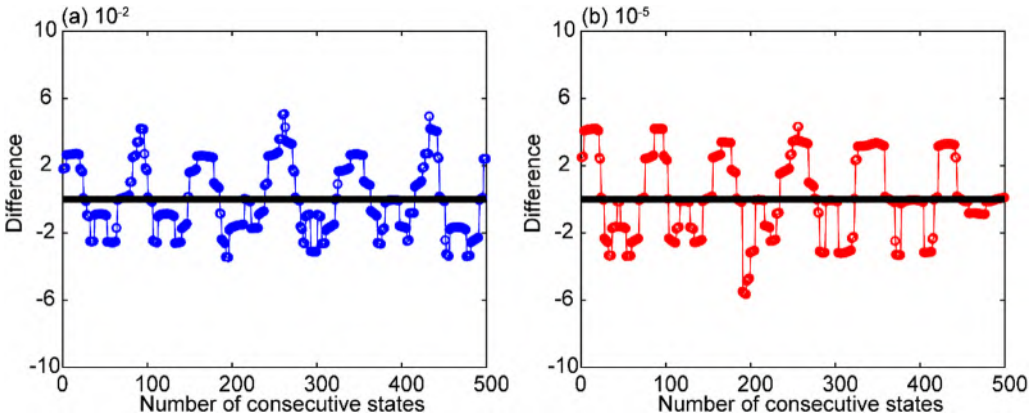

Fig. 9. Difference in local predictabilities for each state from initial condition and parameter errors for a trajectory of 500 states with error magnitudes of (a) 10^{-2} and (b) 10^{-5}. The black line indicates no difference.

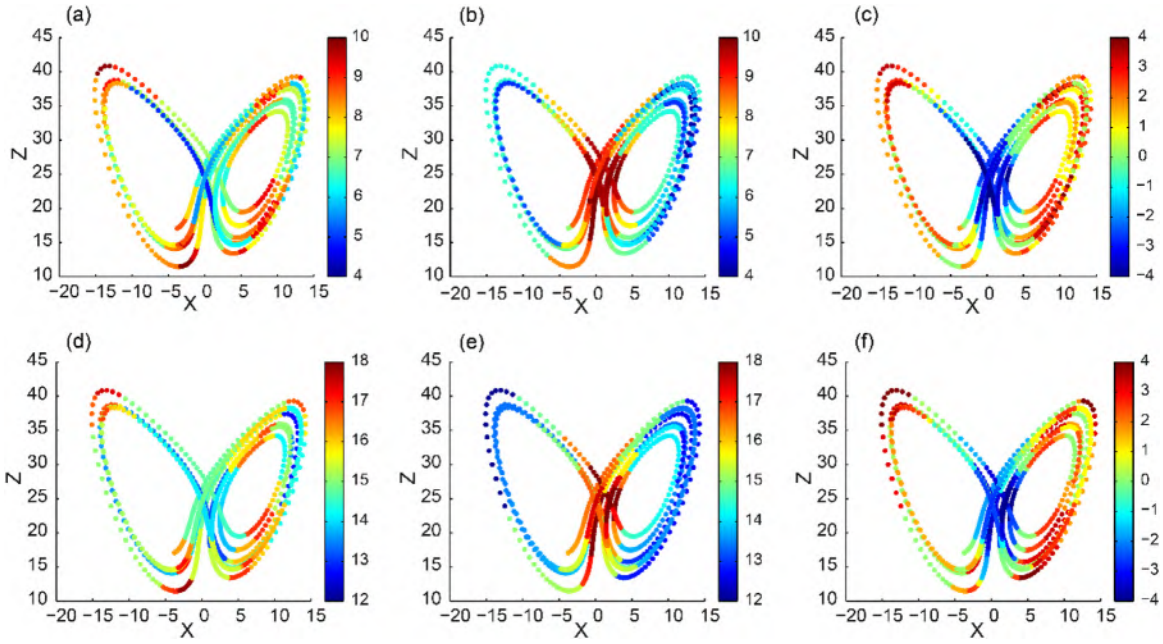

Fig. 10. Spatial distributions of local predictability limits projected on the X–Z plane of the Lorenz attractor with initial condition and model uncertainty magnitudes of (a–c) 10^{-2} and (d–f) 10^{-5}. The left panels are with only initial condition errors in the system, the middle panels are with only model errors in the system, and the right panels are the difference between the predictability limits induced by initial condition and model errors.

jority. This demonstrates that the forecast time in the initial condition uncertainty scenario ranges from 0 to 4 time units longer than in the model uncertainty scenario, both of which have the same uncertainty magnitude in this region. In a minority of regions in the "butterfly wing", the initial condition and model uncertainties have the same influence on local predictability, and the forecast times are the same regardless of which type of uncertainty is present. In summary, the regime transition region is always sensitive to initial condition uncertainty, and the "butterfly wing" regions are generally sensitive to model uncertainty. It may be differing dynamics related to initial condition and model uncertainties that results in this interesting phenomenon. We next explore this possibility. The 500 consecutive states shown in Fig. 8a move periodically back and forth through the two regimes, indicating the periodic movement of states through regions with different sensitivities to uncertainty. As a result, the differences between the local predictability limits of consecutive states on the attractor induced by initial condition and model uncertainties change periodically.

Evans et al. [20] classified the Lorenz attractor into two weather regimes. As described above, in the regime transition region, the local predictabilities of states are more sensitive to initial condition uncertainty than they are to model uncertainty. This suggests that more attention should be paid to reducing initial condition uncertainty during transitions between the two regimes. In this way, forecast skill can be effectively improved. During either regime, the local predictabilities are more sensitive to model uncertainty. During these periods, the focus should be on improving the accuracy of the model to improve forecasts.

In the real atmospheric system, the initial condition and model uncertainties are both present [54]. Consequently, we designed another experiment to investigate the impacts on local predictability limits of a scenario in which both uncertainties are present in the model. In this scenario, the state and three parameters are all imperfect. A group of error vectors is superimposed on $\boldsymbol{x}(t_0)$, $\boldsymbol{y}(t_0)$, $\boldsymbol{z}(t_0)$, σ, r, and b. Then, the perfect model is integrated for 5000 time steps from the true state $(\boldsymbol{x}(t_0), \boldsymbol{y}(t_0), \boldsymbol{z}(t_0))$ as a true run, and the imperfect model for 5000 time steps from the imperfect state

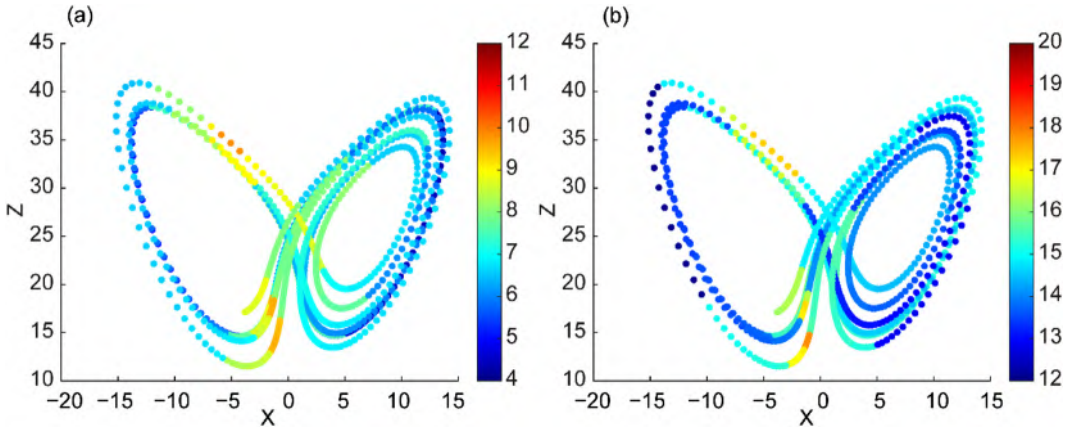

Fig. 11. Spatial distributions of local predictability limits projected on the X–Z plane in the scenario with initial condition and model uncertainties both present in the Lorenz model. The magnitudes of initial condition and model uncertainties are (a) 10^{-2} and (b) 10^{-5}, respectively.

($\boldsymbol{x}'(t_0)$, $\boldsymbol{y}'(t_0)$, $\boldsymbol{z}'(t_0)$) as a forecast run. Using the NLLE method, the local predictability limit of state ($\boldsymbol{x}(t_0)$, $\boldsymbol{y}(t_0)$, $\boldsymbol{z}(t_0)$) can be determined quantitatively when the initial condition and model uncertainties are both present in the model.

Fig. 11 shows the spatial distributions of local predictability limits in the scenario where both uncertainties are present in the Lorenz model. As shown in Fig. 11, the local predictability limits are, on the whole, lower that those induced by only one type of uncertainty existing in the model, indicating that the combination of initial condition and model uncertainties has a greater impact on the predictability of the Lorenz model. When only the initial condition uncertainty is present in the model, the local predictability limits are generally higher in the "butterfly wing" regions, but lower in the regime transition region. The spatial distributions of local predictability limits are inverse when only the model uncertainty is present in the model. However, from Fig. 11, the differences in the local predictability limits of states in different regions are not so large compared with those induced by initial condition or model uncertainties. In our opinion, when both uncertainties are present in the Lorenz model, the respective effects of the initial condition and model uncertainties can offset each other, which decreases the spatial differences induced when only one type of uncertainty is present.

4. Discussion and conclusions

Initial condition and model uncertainties are unavoidable, and are responsible for the loss of atmospheric predictability. The relative effects of the two types of uncertainty on predictability remain uncertain, despite much research being performed on this subject. One reason for this is that the two types of uncertainty are difficult to separate from each other. In this work, we adopt the classic Lorenz model as a surrogate for the atmosphere to study the relative effects of initial condition and model uncertainties on local predictability. In this chaotic model, the initial condition and model uncertainties can not only be separated in idealized experiments, but their respective effects on local predictability can also be studied. The LLE method is practicable only in the scenario with initial errors being infinitesimally small, when the errors grow to a certain size and their evolution is not governed by the linear theory. That is, the LLE method fails to characterize the average growth rates of large errors. The NLLE method has no such limitation and is applicable even with large errors. Therefore, we used the NLLE method to quantify the local predictabilities of states when only initial or model uncertainties are present in the system. The local predictability limits induced by initial condition and model uncertainties can then be determined. A quantitative comparison of the relative effects of initial condition and model uncertainties is obtained by calculating the differences of local predictability limits of the same states induced by the two types of uncertainty with the same magnitude.

First, we compare the growth rates for initial condition and model errors superimposed on different states of the same magnitude. Results show that the relative growth rates of the two types of uncertainty vary with iteration step and state. The corresponding growth of initial condition and model uncertainties also changes with iteration step and state. For different states, the time required for initial condition uncertainty to reach saturation can be greater or less than that for model uncertainty, with both uncertainties reaching saturation simultaneously for some states. In addition, the local predictability limits decrease as the magnitudes of the two types of uncertainty increase, suggesting that both types of uncertainty have negative effects on local predictability limits. We also considered the sensitivity of local predictability to each parameter and found that it is most sensitive to parameter b, less sensitive to parameter r, and least sensitive to parameter σ.

To compare quantitatively the relative effects of the two types of uncertainty on local predictability, the differences between the local predictability limits of 500 consecutive states induced by initial condition and model uncertainties are calculated. Results show that the differences fluctuate around zero, indicating the relative effects of initial condition and model uncertainty vary with state. Moreover, the differences change periodically. To determine the cause of this phenomenon, spatial distributions of predictability limits on the Lorenz attractor induced by the two types of uncertainty are evaluated. Distinct inverse spatial distributions of local predictability limits are found to be induced by initial condition and model uncertainties. In the two "butterfly wing" regions of the Lorenz attractor, the local predictability limits induced by initial condition uncertainty are relatively high, whereas the local predictability limits are relatively low in the regime transition region. For model uncertainty, the opposite is true. The local predictability limits are relatively high in the regime transition region but low in the two "butterfly wing" regions of the Lorenz attractor. The spatial distributions of differences between the local predictability limits induced by initial condition and model uncertainties (Fig. 10c and f) are less than zero, and are approximately −4 in the regime transition region, suggesting forecasts can be 4 time units longer in the model uncertainty scenario than in the initial condition uncertainty scenario, both of which are of the same magnitude. In the two "butterfly wing" regions of the Lorenz attractor, the differences range from 0 to 4, with zero values accounting for only

a minority of areas. This suggests that we can forecast up to four time units longer in most regions when model uncertainty but not initial condition uncertainty is present. In a minority of areas, the forecast times are the same for both types of uncertainty. Therefore, the regime transition region is sensitive to initial condition uncertainty, whereas the "butterfly wing" regions are sensitive to model uncertainty. The different sensitivities of these regions on the attractor to initial condition and model uncertainties result in periodic changes in the differences in local predictability limits. It may be differing dynamics related to the two types of uncertainty that leads to the different sensitivities of states in the same region to initial condition and model uncertainties. However, this needs further study.

The varying regional sensitivity to initial condition and model uncertainty indicates that reducing the initial condition uncertainty during the transition of two regimes may improve forecast skill. During either regime, the focus should be on reducing model uncertainty to improve forecast skill. We also studied the impacts of initial condition and model uncertainties on local predictability limits when both uncertainties are present. The results indicate that differences in the spatial distribution of the local predictability limits are not large compared with those induced by initial condition or model uncertainty. It is the combined effects of initial condition and model uncertainties that reduce the spatial differences induced by only one type of uncertainty.

Initial condition and model uncertainties have different effects on local predictability, it is of great significance to investigate their relative roles with respect to local predictability. The Lorenz model used in this work, which has three variables, is much simpler than the sophisticated atmospheric and climate models with a high number of degrees of freedom. Compared with the Lorenz model, the variability of the local Lyapunov exponents is reduced in the sophisticated atmospheric and climate models. Nicolis et al. [55] pointed out that a super-exponential growth of errors would arise when the variability is large. Because of the low variability of local Lyapunov exponents in sophisticated atmospheric and climate models, the impact of variability on error saturation would in principle be lower than in the Lorenz system. As for the relative contributions of initial condition and model uncertainty to predictability in sophisticated atmospheric and climate models, the present results support the view of Lorenz [41]. In short-range forecasts, the initial condition has a greater impact on local predictability, whereas the model uncertainty will play a more important role in long-range forecasts. To verify this point, sophisticated atmospheric and climate models will be needed to study the relative roles of initial condition and model uncertainties in future work. Nevertheless, our theoretical results presented here are instructive and worthy of further study.

Declaration of Competing Interest

The authors declare that they have no known competing financial interests or personal relationships that could have influenced the work reported in this paper.

CRediT authorship contribution statement

Xuan Li: Conceptualization, Methodology, Software, Validation, Writing - original draft. **Ruiqiang Ding:** Conceptualization, Methodology, Writing - review & editing. **Jianping Li:** Conceptualization, Methodology, Writing - review & editing.

Acknowledgments

This work was jointly supported by the National Natural Science Foundation of China (Grant No. 41790474), and the National Program on Global Change and Air–Sea Interaction (GASI-IPOVAI-03, GASI-IPOVAI-06).

References

[1] Anthes RA. Data assimilation and initialization of hurricane prediction models. J Atmos Sci 1974;31:702–19.
[2] Bauer P, Buizza R, Cardinali C, Thepaut JN. Impact of singular-vector-based satellite data thinning on NWP. Q J R Meteor Soc 2011;137:286–302.
[3] Becker E, van den Dool H. Probabilistic seasonal forecasts in the North American multimodel ensemble: a baseline skill assessment. J Clim 2016;29:3015–26.
[4] Campins J, Navascues B, Santos C, Amo-Baladron A. Influence of targeted observations on short-term forecasts of high-impact weather events in the Mediterranean. Nat Hazard Earth Sys 2013;13:2891–910.
[5] Chou JF. Predictability of the atmosphere. Adv Atmos Sci 1989;6:335–46.
[6] Chu PC. Two kinds of predictability in the Lorenz system. J Atmos Sci 1999;56:1427–32.
[7] Collins M, Allen MR. Assessing the relative roles of initial and boundary conditions in interannual to decadal climate predictability. J Clim 2002;15:3104–9.
[8] Dalcher A, Kalnay E. Error growth and predictability in operational ECMWF forecasts. Tellus A 1987;39:474–91.
[9] Ding RQ, Li JP. Nonlinear finite-time Lyapunov exponent and predictability. Phys Lett A 2007;364:396–400.
[10] Ding RQ, Li JP. The temporal-spatial distributions of weather predictability of different variables. Acta Meteol Sin 2009;3:343–54.
[11] Ding RQ, Li JP. Application of nonlinear error growth dynamics in studies of atmospheric predictability. Acta Meteol Sin 2009;2:241–9.
[12] Ding RQ, Li JP, Kyung-Ja HA. Nonlinear local Lyapunov exponent and quantification of local predictability. Chin Phys Lett 2008;25:1919–22.
[13] Ding RQ, Li JP, Seo KH. Predictability of the Madden–Julian Oscillation estimated using observational data. Mon Weather Rev 2010;138:1004–13.
[14] Ding RQ, Li JP, Li BS. Determining the spectrum of the nonlinear local Lyapunov exponents in a multidimensional chaotic system. Adv Atmos Sci 2017;34:1027–34.
[15] Ding RQ, Li JP, Zheng F, Feng J, Liu DQ. Estimating the limit of decadal-scale climate predictability using observational data. Clim Dyn 2015;46:1563–80.
[16] Downton RA, Bell RS. The impact of analysis differences on a medium-range forecast. Meteor Mag 1988;117:279–85.
[17] Duan WS, Huo ZH. An approach to generating mutually independent initial perturbations for ensemble forecasts: orthogonal conditional nonlinear optimal perturbations. J Atmos Sci 2016;73:997–1014.
[18] Duan WS, Hu JY. The initial errors that induce a significant "spring predictability barrier"" for El Nino events and their implications for target observation: results from an earth system model. Clim Dynam 2016;46:3599–615.
[19] Duan WS, Mu M, Wang B. Conditional nonlinear optimal perturbations as the optimal precursors for El Nino–Southern Oscillation events. J Geophys Res-Atmos 2004;109:D23105. doi:10.1029/2004JD004756.
[20] Evans ECoauthors. Rise undergraduates find that regime changes in Lorenz's model are predictable. Bull Amer Meteor Soc 2004;85:520–4.
[21] Farrell BF. Small error dynamics and the predictability of atmospheric flows. J Atmos Sci 1990;47:2409–16.
[22] Feng J, Ding RQ, Liu DQ, Li JP. The application of nonlinear local Lyapunov vectors to ensemble predictions in Lorenz systems. J Atmos Sci 2014;71:3554–67.
[23] Gao XQ, Feng GL, Dong WJ, Chou JF. On the predictability of chaotic systems with respect to maximally effective computation time. Acta Meteor Sin 2003;19:134–9.
[24] Goerss JS. Tropical cyclone track forecasts using an ensemble of dynamical models. Mon Weather Rev 2000;128:1187–93.
[25] Goswami BN, Shukla J. Predictability of a coupled ocean–atmosphere model. J Clim 1991;4:3–22.
[26] Harrison MSJ, Palmer TN, Richardson DS, Buizza R. Analysis and model dependencies in medium-range ensembles: two transplant case-studies. Q J Roy Meteor Soc 1999;125:2487–515.
[27] Houtekamer PL. Variation of the predictability in a low-order spectral model of the atmospheric circulation. Tellus A 1991;43:177–90.
[28] Kirtman BP, Min D. Multimodel ensemble ENSO prediction with CCSM and CFS. Mon Weather Rev 2009;137:2908–30.
[29] Lacarra JF, Talagrand O. Short-range evolution of small perturbations in a barotropic model. Tellus A 1988;40:81–95.
[30] Leith CE. Objective methods for weather prediction. Annu Rev Fluid Mech 1978;10:107–28.
[31] Li JP, Ding RQ. Temporal–spatial distribution of atmospheric predictability limit by local dynamical analogs. Mon Weather Rev 2011;139:3265–83.
[32] Li JP, Ding RQ. Temporal–spatial distribution of the predictability limit of monthly sea surface temperature in the global oceans. Int J Climatol 2013;33:1936–47.
[33] Li JP, Feng J, Ding RQ. Attractor radius and global attractor radius and their application to the quantification of predictability limits. Clim Dyn 2017;51:2359–74.
[34] Li X, Ding RQ, Li J. Determination of the backward predictability limit and its relationship with the forward predictability limit. Adv Atmos Sci 2019;36:669–77.
[35] Lorenz EN. Deterministic nonperiodic flow. J Atmos Sci 1963;20:130–41.

[36] Lorenz EN. A study of the predictability of a 28-variable atmospheric model. Tellus 1965;17:321–33.
[37] Lorenz EN. Atmospheric predictability as revealed by naturally occurring analogues. J Atmos Sci 1969;26:636–46.
[38] Lorenz EN. The predictability of a flow which possesses many scales of motion. Tellus 1969;21:289–307.
[39] Lorenz EN. The physical bases of climate and climate modelling. Clim Predict. 1975;16:132–6 WMO.
[40] Lorenz EN. Irregularity: a fundamental property of the atmosphere. Tellus A 1984;36:98–110.
[41] Lorenz EN. Effects of analysis and model errors on routine. In: *Proceeding ECMWF Seminar on Ten Years of Medium Range Weather Forecasting*. ECMWF; 1989. p. 115–28.
[42] Lorenz EN. Predictability: a problem partly solved. In: *Proceeding ECMWF Seminar on Predictability*, I. ECMWF; 1996. p. 1–18.
[43] Lorenz EN. A look at some details of the growth of initial uncertainties. Tellus A 2005;57:1–11.
[44] Majumdar SJ, Coauthors. Targeted observations for improving numerical weather prediction: an overview, 15. World Weather Research Programme/THORPEX Publication; 2011. p. 37.
[45] Mittal AK, Singh UP, Tiwari A, Dwivedi S, Joshi MK, Tripathi KC. Short-term predictions by statistical methods in regions of varying dynamical error growth in a chaotic system. Meteor Atmos Phys 2015;127:457–65.
[46] Molteni F, Palmer TN. Predictability and finite-time instability of the northern winter circulation. Q J R Meteor Soc 1993;119:269–98.
[47] Mu M, Zhang Z. Conditional nonlinear optimal perturbations of a two-dimensional quasigeostrophic model. J Atmos Sci 2006;63:1587–604.
[48] Mu M, Jiang ZN. Similarities between optimal precursors that trigger the onset of blocking events and optimally growing initial errors in onset prediction. J Atmos Sci 2011;68:2860–77.
[49] Mu M, Duan WS, Wang B. Conditional nonlinear optimal perturbation and its applications. Nonlinear Process Geophys 2003;10:493–501.
[50] Mu M, Zhou FF, Wang HL. A method for identifying the sensitive areas in targeted observations for tropical cyclone prediction: Conditional nonlinear optimal perturbation. Mon Weather Rev 2009;137:1623–39.
[51] Mu M, Duan WS, Chen DK, Yu WD. Target observations for improving initialization of high-impact ocean-atmospheric environmental events forecasting. Natl Sci Rev 2015;2:226–36.
[52] Mukougawa H, Kimoto M, Yoden S. A relationship between local error growth and quasi-stationary states: case study in the Lorenz system. J Atmos Sci 1991;48:1231–7.
[53] Nese JM. Quantifying local predictability in phase space. Physica D 1989;35:237–50.
[54] Nicolis C, Perdigao R, Vannitsem S. Dynamics of prediction errors under the combined effect of initial condition and model errors. J Atmos Sci 2009;66:766–78.
[55] Nicolis C, Vannitsem S, Royer J-F. Short-range predictability of the atmosphere: mechanisms for superexponential error growth. Q J R Meteor Soc 1995;121:705–22.
[56] Orrell D, Smith L, Barkmeijer J, Palmer TN. Model error in weather forecasting. Nonlinear Process Geophys 2001;8:357–71.
[57] Palmer TN. Extended-range atmospheric prediction and the Lorenz model. Bull Am Meteor Soc 1993;74:49–65.
[58] Palmer TN. Predicting uncertainty in forecasts of weather and climate. Rep Prog Phys 2000;63:71–116.
[59] Palmer TN, Buizza R, Molteni F, Chen YQ, Corti S. Singular vectors and the predictability of weather and climate. Philos T R Soc A 1994;348:459–75.
[60] Palmer TNCoauthors. Development of a European multimodel ensemble system for seasonal-to-interannual prediction (DEMETER). Bull Am Meteor Soc 2004;85:853–72.
[61] Richardson DS. The relative effect of model and analysis differences on ECMWF and UKMO operational forecast. In: *Proceeding ECMWF Workshop on Predictability*, Reading. United Kingdom: ECMWF; 1997. p. 363–72.
[62] Shukla J. Predictability. Adv Geophys 1985;28B:87–122.
[63] Simmons AJ, Hollingsworth A. Some aspects of the improvement in skill of numerical weather prediction. Q J R Meteor Soc 2002;128:647–77.
[64] Singh B, Cash B, Kinter JL. Indian summer monsoon variability forecasts in the North American multimodel ensemble. Clim Dyn 2019;53:7321–34.
[65] Sun GD, Peng F, Mu M. Uncertainty assessment and sensitivity analysis of soil moisture based on model parameter errors—results from four regions in China. J Hydrol 2017;555:347–60.
[66] Thompson PD. Uncertainty of initial state as a factor in the predictability of large scale atmospheric flow patterns. Tellus 1957;9:275–95.
[67] Trevisan A. Impact of transient error growth on global average predictability measures. J Atmos Sci 1993;50:1016–28.
[68] Trevisan A, Legnani R. Transient error growth and local predictability: a study in the Lorenz system. Tellus A 1995;47:103–17.
[69] Vannitsem S, Toth Z. Short-term dynamics of model errors. J Atmos Sci 2002;59:2594–604.
[70] Vannitsem S, Lucarini V. Statistical and dynamical properties of covariant Lyapunov vectors in a coupled atmosphere–ocean model-multiscale effects, geometric degeneracy, and error dynamics. J Phys A-Math Theor 2016;49:31.
[71] Wang XG, Barker DM, Snyder C, Hamill TM. A hybrid ETKF–3DVAR data assimilation scheme for the WRF model. Part I: Observing system simulation experiment. Mon Weather Rev 2008;136:5116–31.
[72] Yadav RS, Dwivedi S, Mittal AK. Prediction rules for regime changes and length in a new regime for the Lorenz model. J Atmos Sci 2005;62:2316–21.
[73] Yamane S, Yoden S. Finite-time evolution of small perturbations superposed on a chaotic solution: Experiment with an idealized barotropic model. J Atmos Sci 2001;58:1066–78.
[74] Yoden S, Nomura M. Finite-time Lyapunov stability analysis and its application to atmospheric predictability. J Atmos Sci 1993;50:1531–43.
[75] Yu YS, Mu M, Duan WS. Does model parameter error cause a significant spring predictability barrier for El Niño events in the Zebiak–Cane model? J Clim 2012;25:1263–77.
[76] Zhang F, Odins AM, Nielsen-Gammon JW. Mesoscale predictability of an extreme warm-season precipitation event. Weather Forecast 2006;21:149–66.
[77] Zhang FQ, Snyder C, Rotunno R. Mesoscale predictability of the "surprise" snowstorm of 24–25 January 2000. Mon Weather Rev 2002;130:1617–32.
[78] Zhang FQ, Weng YH, Gamache JF, Marks FD. Performance of convection-permitting hurricane initialization and prediction during 2008–2010 with ensemble data assimilation of inner-core airborne Doppler radar observations. Geophys Res Lett 2011:L15810. doi:10.1029/2011GL048469.
[79] Zhu HY, Thorpe A. Predictability of extratropical cyclones: The influence of initial-condition and model uncertainties. J Atmos Sci 2006;63:1483–97.
[80] Ziehmann C, Smith LA, Kurths J. Localized Lyapunov exponents and the prediction of predictability. Phys Lett A 2000;271:237–51.